




## Atomistic insight into the initial stage of graphene formation on SiC(0001) surfaces

Mauro Boero <sup>1,2,\*</sup>, Fumihiro Imoto <sup>2</sup>, and Atsushi Oshiyama <sup>2,†</sup>

<sup>1</sup>University of Strasbourg, Institut de Physique et Chimie des Matériaux de Strasbourg,  
CNRS, UMR 7504 23 rue du Loess, F-67034 Strasbourg, France

<sup>2</sup>Institute of Materials and Systems for Sustainability, Nagoya University, Nagoya 464-8603, Japan



(Received 19 May 2022; revised 5 August 2022; accepted 13 September 2022; published 30 September 2022)

We present an atomistic insight into the processes leading to the formation of graphene on SiC(0001) surfaces by resorting to first-principles molecular dynamics empowered by free-energy sampling methods. Based on the experimental surface, consisting of terraces bordered by a sequence of steps, we find that Si atoms are dislodged from step edges and migrate toward more stable sites on the terrace, leaving behind C atoms carrying unsaturated chemical bonds. Our investigations reveal that subsequent Si atoms removal acts as a trigger to the formation of stable C-C bonds among these unsaturated C sites. This process eventually leads to the formation of C clusters which merge into larger structures with the typical pattern of graphene flakes. Specifically, a C<sub>6</sub> ring formed during our simulations, assumes the typical hexagonal structure of graphene, becoming a precursor of larger graphene nanostructures. The characterization of the mechanisms and related free-energy landscapes provide an insight into the fundamental processes responsible for the realization of ordered C-based building blocks of graphene on the SiC(0001) surface.

DOI: [10.1103/PhysRevMaterials.6.093403](https://doi.org/10.1103/PhysRevMaterials.6.093403)

### I. INTRODUCTION

Graphene has a consolidated background as an innovative two-dimensional (2D) material since its pioneering age [1,2]. This is mainly due to the intrinsic low cost of carbon as a constituting chemical element and because of the peculiar electronic and mechanical properties [3] of the graphene phase. This has boosted also novel applications in electronic devices [4,5] and represents still a premier 2D material worldwide for present and next-generation electronics. Several methods have been proposed to produce graphene sheets [6–8]. Among all these innovative possibilities, an emerging technology consists in the thermal decomposition of silicon carbide (SiC) [9–11]. The major advantage of this technique is the possibility of growing graphene directly on a semiconducting substrate, thus avoiding the difficult step of extracting and transferring graphene sheets on a substrate, which is a delicate stage responsible for inducing defects and permanent damage of the pristine graphene layer. From a scientific standpoint, the formation of graphene from a SiC crystal, possibly accompanied by a selective removal of Si atoms and subsequent condensation of C atoms, is still an unexplored issue. To date, the mechanism responsible for such a graphene formation on SiC surfaces is far from being understood and this is a stumbling block to the realization of high-quality graphene flakes and layers on SiC.

An additional difficulty is the empirical evidence that the grown graphene is strongly dependent on the SiC crystal-plane orientation of the exposed surface on which the

nucleation and growth occur. One of the best possible orientations has been identified as the (0001) surface. On this specific surface, a monolayer or a few layers of graphene have been produced upon proper tuning of the growth condition, especially temperature and pressure [10,12,13]. Concerning the early stages of the growth process, high-resolution transmission electron microscopy experiments have shown that graphene starts forming by nucleation at the (11 $\bar{2}$ *n*) nanofacets ( $n \approx 12$ ), then the growth proceeds toward the terrace [14]. Experiments have also evidenced that graphene structures grown on the (0001) surface consist of a  $13 \times 13$  elementary graphene cell. This particular size is commensurate with a  $6\sqrt{3} \times 6\sqrt{3}$  SiC supercell [15–19] and provides a reliable model for our computational studies. Furthermore, accurate scanning tunneling microscopy and spectroscopy investigations [20,21] have evidenced the importance of step edges as active sites for the graphene formation process.

On a theoretical standpoint, one of the most recent and thorough investigations of the Si removal process from SiC surfaces has been reported by Zhang and van Duin [22] using long-lasting classical molecular dynamics (CMD) simulations. These were made possible by the use of an *ad hoc* developed reactive force field. However, the capability of describing detailed features of possibly new chemical reactions during the Si removal and the subsequent graphene formation is not assured in any *ad hoc* force field. The CMD simulations have also provided evidence for nucleation of C multiring structures at the step edge upon removal of Si atoms [23]. This initial multiring C cluster displays a pentaheptagonal structure rather than a hexagonal one, as expected for a graphene precursor [24]. CMD studies also indicated that the progressive evolution of an initial multiring cluster toward graphene might actually occur [25]. However, the

\*mauro.boero@ipcms.unistra.fr

†oshiyama@imass.nagoya-u.ac.jp

capability of describing detailed features of possibly new chemical reactions during the Si removal and the subsequent graphene formation is not assured in any *ad hoc* force field. An accurate description of these unknown chemical reactions is possible only if the electronic structure evolution and bonding modifications are properly accounted for. This is ensured by first-principle dynamical approaches within the density functional theory (DFT) [26].

Former DFT-based total-energy calculations and structural optimization have shown that the bottom layer of the graphene sheet has a strong interaction with the SiC substrate buffer layer [27,28]. Then, graphene is formed on a SiC surface provided that a sufficient amount of C atoms is present [29,30], and the aggregation of C atoms at the step edge is indeed responsible for a minimization of the total energy of the system [30]. Nonetheless, these static DFT calculations shed only little light on the actual atomistic mechanism of the graphene formation. DFT-based dynamical simulations for the well-identified step structures where the initial stage of the graphene formation occurs are indispensable, yet still missing.

The structural identification of surface steps of SiC(0001) was targeted in our former work [31]. DFT calculations within a hybrid generalized-gradient approximation including the exact exchange on the exchange-correlation functional have clarified that the observed  $(11\bar{2}n)$  nanofacets where the graphene is initially formed are made of bunching of single-bilayer steps [32,33]. The single-bilayer steps show five distinct patterns on SiC(0001) and the structure of each bilayer step edge and its energetics have been recently unraveled by DFT calculations [34,35]. Namely, the step edge where an initial stage of the graphene formation begins has been identified as a particular step edge, termed SC step. In the SC step edge, an upper Si and a lower C in the top bilayer appear at the step edge. These edge atoms are undercoordinated and, as such, preferred active sites for graphene formation. A plausible reaction pathway for the initial stage of graphene formation is likely to be a selective detachment of the edge Si atoms. In this specific context, Imoto *et al.* [31] found that the Si atom at the SC step edge is selectively detached from the step edge toward the surface terrace and the subsequent formation of C-C bonds makes the reaction exothermic. A direct sublimation of the dislodged Si into the gas phase would be energetically unfavorable according to our calculations, being the energetic cost is considerably larger than 5 eV. Hence, the identified Si detachment from the step edge to the nearby terrace is the most favorable pathway compared with other possibilities such as an exchange reaction where fourfold coordinated subsurface C emerges on the surface, since the edge Si is threefold coordinated, or pinned by a weak Si-Si bond even after the reconstruction [34,35]. Given this scenario, in this work we investigate and clarify the various stages of the actual reaction pathways for the selective Si detachment from the step edge and then explore subsequent reactions leading to the formation of a graphene seed via free-energy enhanced first-principles molecular dynamics (FPMD).

The scope of the present study is thus to overcome difficulties and limitations of CMD and static DFT total-energy optimizations in tackling this far from trivial chemical process. Specifically, we provide an insight into the atomistic mechanism regulating the graphene formation, accounting

for the subtle electronic structure changes and the interplay between Si detachment from the step edge (or desorption hereafter) and subsequent C bond formation, working out reaction pathways and related free-energy landscapes. To this aim, we resort to FPMD simulations within the Car-Parrinello (CPMD) framework [36] as implemented in the developers version 4.3 [37], complemented by metadynamics (MTD) [38,39] for the exploration of the activated processes and associated free-energy profiles. The C-C bond formation triggered by Si detachment at the step edge is presented and discussed in Secs. III A and III B. In Sec. III C we extend our study to the case of multiple Si atoms removal leading to the formation of C structures as precursors for graphene monolayers.

## II. METHODS

According to the guidelines proposed by available experiments, we focused on the nanofacet consisting of bunched single-bilayer steps [32,33]. On this morphology, we study the reactions occurring at a single-bilayer step edge. In particular, we consider the desorption of an initial Si atom from a pristine step edge. Subsequently, we investigate the desorption of additional Si leading to the formation of C-C bonds. Our simulated stepped surface consists in a periodically repeated slab model in which the top surface of the slab presents an upper and a lower terrace, bordered by a single-bilayer step. The periodicity of this structural unit goes along the lateral dimensions, as a periodic-array model or a trench-shape model [35]. The bottom of the slab is terminated by H atoms to remove fictitious dangling bonds and then mimic a semi-infinite substrate [40]. Each atomic slab is separated vertically from its images by a vacuum with a thickness of more than 8 Å. The SiC motif targeted here is a  $4H$  structure in which we choose the upper (lower) terrace as the cubic (hexagonal) surface. We underscore that an alternative stacking sequence of the bilayers along the [0001] direction, carrying a hexagonal upper terrace, provides results identical to those presented here. Following the typical experimental situation using the  $[11\bar{2}0]$ -inclined [0001] surface, the step edge is parallel to the  $[1\bar{1}00]$  direction and its structure is labeled as SC [34,35]. We use two different supercells. The terrace size is  $7 \times 2\sqrt{3}$  in the first one and is  $9 \times 3\sqrt{3}$  in the second one. Each contains five or four bilayers or two or three bilayers. As a result, the former and the latter supercells contain 280 and 336 atoms, respectively. The larger supercell is used to study the processes leading to the clustering of C atoms, precursors of graphene formation. The parameters used here are essentially identical to those of our previous work [31], which give lattice constants of  $4H$ -SiC,  $a = 3.09$  Å and  $c = 10.03$  Å being only 0.67% and 0.78% larger than the experimental values, respectively. We use our theoretical equilibrium structural parameters and allow all the atoms except for the bottom atoms in the slab to evolve freely during all the simulations. Furthermore, we checked for residual pressure on our simulated systems during the initial (unbiased) FPMD equilibration run by computing the stress tensor of our simulation cell. As shown in Fig. S1 of the Supplemental Material (SM) [41–43], no residual stress or strain affects our model system.

In all canonical  $NVT$  simulations, the temperature (300 K) is controlled by a Nosé-Hoover thermostat chain [44–47]. For the treatment of the exchange and correlation interaction in our DFT approach, we adopt the generalized-gradient approximation [48] proposed by Perdew, Burke, and Ernzerhof, complemented by the Grimme’s van der Waals corrections [49] to account for long-range dispersion forces. The core-valence interaction is described by norm-conserving pseudopotentials [50], whereas valence electrons are treated explicitly and their orbitals expanded on a plane-wave basis set with a cutoff energy of 70 Ry. The Brillouin zone sampling is limited to the  $\Gamma$  point because of the sufficiently large lateral size. An electron fictitious mass of 340 a.u. and an integration time step of 4.0 a.u. ( $9.67 \times 10^{-5}$  ps) for the CPMD equations of motion ensured a good control of the conserved quantities and numerical stability of the dynamics.

The Car-Parrinello molecular dynamics is used here just as a driver for the exploration of the free-energy landscape as explained in detail in all the related literature [38,39,51,52]. Reactive processes and free-energy sampling are then the result of the joint use of the CPMD method empowered by the variational formulation of MTD [39] in which the free energy  $F(\mathbf{s})$  spanned by the collective variables (CVs)  $\mathbf{s} = (s_1, s_2, \dots)$  is reconstructed *a posteriori* according to the formula

$$\lim_{t \rightarrow \infty} V(\mathbf{s}, t) = -F(\mathbf{s}) + \text{constant}. \quad (1)$$

Here  $V(\mathbf{s}, t)$  is the time-evolving potential in which penalty functions filling the local minima are accumulated during the MTD. Further details can be found in the quoted literature and the specific CVs used in the present work to sample each reaction pathway will be given explicitly in the next paragraphs whenever needed to support the discussion. An additional speedup for MTD was achieved by the use of multiple walkers [53].

### III. RESULTS AND DISCUSSION

#### A. First Si desorption from the step edge

The formation of carbon structures in a SiC matrix has to start necessarily from the removal of Si atoms from their initial positions in which they form chemical bonds with C atoms. To this aim, we started by investigating the desorption of Si from the step edge within the MTD framework. In this case, we used as a CV the distance between a desorbing Si and the center of mass (COM) of a site defined by three C atoms exposed on the lower terrace as sketched in Fig. 1, where the desorbed Si and the COM site are indicated by a red and black sphere, respectively. In the figure, the local minima explored and the transition state identified along this reaction path are indicated by the labels (A), (B), (C), and (TS) along the free-energy profile.

Starting from the initial configuration (A), the system overcomes an energy barrier of about 1.38 eV realizing the transition state (TS) ( $TS_{A \rightarrow B}$  in Fig. 1), and after visiting a metastable minimum (B) in which the desorbing Si is located on top of a C atom on the lower terrace, arrives at the final minimum (C) at slightly higher energy and labeled as an H3 site. The largest free-energy difference between the

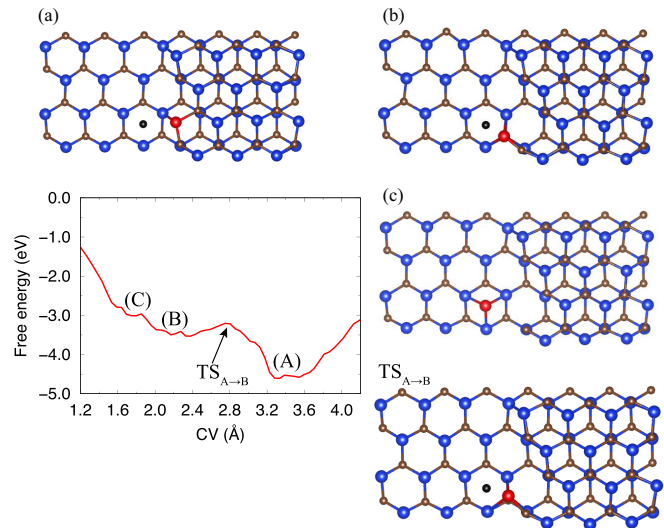


FIG. 1. Free-energy profile of Si desorption from the step edge and major relevant configurations. The color code for the atoms is blue for Si and brown for C. The bottom three atomic layers are not shown for clarity. The collective variable (see text for details) is the distance between a desorbing Si (red sphere) and the center of mass (black sphere) of the lower terrace site formed by three C atoms.

(meta)stable and transition-state configurations is the rate-determining barrier of the overall process. According to our MTD estimations, the TS is characterized by a free-energy barrier  $\Delta F(TS_{A \rightarrow B} - A) = 1.38$  eV. This reaction pathway is in agreement with our former DFT-based study [31] and corroborates the static picture provided there. The initial state is located in a low energetic basin of the free-energy profile if compared to the final state (C), indicating that this process is endothermic. We can then infer that this initial stage of the whole reaction, which leads eventually to the graphene formation, is insufficient to provide a full picture of the whole complex process.

#### B. Subsequent Si desorption from the step edge

##### 1. Formation of C-C chemical bond

A desorbed Si atom, which eventually is dislodged to a nearby terrace, can diffuse on the SiC surface with an activation barrier significantly smaller than other barriers characterizing its desorption or the C clustering [31]. For this reason, to investigate the subsequent steps toward the graphene formation we placed the firstly desorbed Si on an H3 site sufficiently far away from the step edge. This gives enough room for a second Si desorption and subsequent displacement to the lower terrace. Starting from these conditions, we performed a MTD to explore the possibilities of both Si desorption from the step edge and C-C formation. To this aim, we selected two CVs. One CV is the distance between the desorbing Si atom (green Si in Fig. 2) and the COM of three C atoms on the lower terrace (site 1, black sphere in Fig. 2); this COM point is analogous to the one in the former MTD simulation. The second CV, instead, is the distance between the edge C atom (magenta C in Fig. 2) and the COM of three C atoms on the upper terrace (site 2 just beneath the green Si



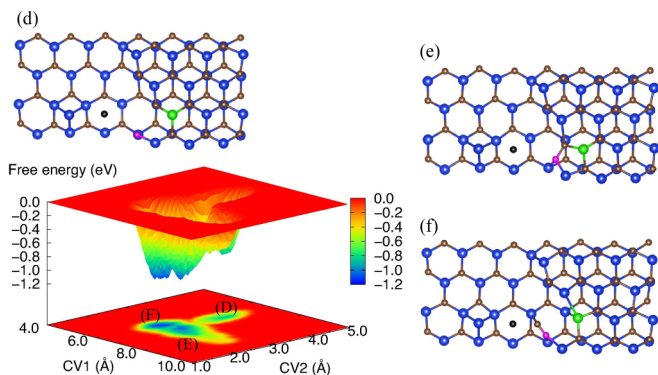


FIG. 2. Free-energy landscape for a second Si desorption from the step edge, accompanied by the formation of a C-C bond and related stable configurations. The two CVs used are the distance between the desorbing Si atom (green sphere) and the COM of three C atoms on the lower terrace (site 1, black sphere), and the distance between the edge C atom (magenta sphere) and the COM of three C atoms on the upper terrace (site 2 underneath the green sphere). One C-C bond is formed in (E) and a C-C and a Si-Si bond appear in (F).

in Fig. 2). This is likely to be the region in which a C atom has the possibility to form C-C chemical bonds.

The initial configuration labeled as (D), evolves toward a metastable state (E) before eventually finding a more stable minimum (F). In (D), the edge C atom (magenta C) is twofold coordinated to Si. In (E), this C atom becomes threefold coordinated to Si and C. In (F), the coordination number of a C atom bonded to the magenta C is smaller than that in (E) by one. On the other hand, the Si shown in green is fourfold coordinated in (F), whereas it is threefold coordinated in (E). In this process, we could identify two transition states,  $TS_{D \rightarrow E}$  and  $TS_{E \rightarrow F}$ , namely, the free-energy barriers to be overcome to go from (D) to (E) and from (E) to (F), respectively. The structures  $TS_{D \rightarrow E}$  and  $TS_{E \rightarrow F}$  are almost identical to (D) and (E), respectively, as shown in Fig. S2 of the SM [41]. The reaction pathway from (D) through (E) to (F) via the above transition states, already found in the landscape reported in Fig. 2, is clearly shown in Fig. S3 of the SM along with the corresponding free-energy profile. In Fig. S3 we show the free-energy landscape and the minimum free-energy pathway (path 1 and path 2 in Fig. S3) [41]. The barriers for the reaction along this pathway are  $\Delta F(TS_{D \rightarrow E} - D) = 0.37$  eV and  $\Delta F(TS_{E \rightarrow F} - E) = 0.11$  eV (Fig. S3 of the SM) [41].

## 2. Formation of three C-C bonds

Subsequent formation of additional carbon chemical bonds is a necessary step in graphene precursors. To this aim, we used the former configuration labeled as (F) as a new initial state to explore the free-energy landscape for further formation of C-C bonds. This can be done by using the same CVs used above. The MTD performed with these CVs has shown a barrierless process consisting in the transition from (F) to (F'). The configuration (F') (Fig. 3) is located away from (F) in the phase space spanned by CV1 and CV2. By continuing the MTD simulation using the same CVs, we have

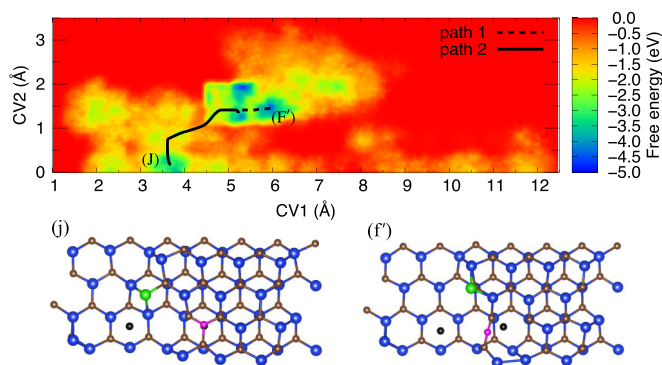


FIG. 3. Free-energy landscape and related stable configurations for the second Si desorption along with the formation of three C-C bonds. Reaction paths 1 and 2 are highlighted as black dashed and solid lines.

found a novel reaction step in which (F') becomes a new stable configuration (J). This final state (J) is characterized by the formation of three C-C bonds (see Figs. S4, S5, and S6 in the SM) [41]. Figure 3 shows the free-energy landscape and the starting and final configurations. The minimum free-energy pathways (path 1 and path 2) are identified by analyzing this landscape. The free-energy profile along the reaction path joining (F') and (J) is shown in Fig. S4 of the SM [41]. Along the reaction pathway from (F') to (J), we have found three metastable states, (G), (H), and (I) (Figs. S3 and S4 in the SM) [41]. In (F'), the edge C (magenta C) is twofold coordinated and the desorbing Si (green Si) is threefold coordinated. In (G), (H), and (I), only the green Si is substantially displaced, where its coordination numbers are 3 in (G), 2 in (H), and 2 in (I). The magenta C finally becomes threefold coordinated, as well as the Si shown in green in (J). These metastable states are separated by four transition states labeled as ( $TS_{F' \rightarrow G}$ ,  $TS_{G \rightarrow H}$ ,  $TS_{H \rightarrow I}$ , and  $TS_{I \rightarrow J}$ ) and the structures are shown in Fig. S6 of the SM [41]. The structures of  $TS_{F' \rightarrow G}$ ,  $TS_{G \rightarrow H}$ ,  $TS_{H \rightarrow I}$ , and  $TS_{I \rightarrow J}$  resemble those of (F'), (G), (H), and (I). The free-energy barriers separating the stable and metastable minima are  $\Delta F(TS_{F' \rightarrow G} - F') = 1.34$  eV,  $\Delta F(TS_{G \rightarrow H} - G) = 1.57$  eV,  $\Delta F(TS_{H \rightarrow I} - H) = 1.26$  eV, and  $\Delta F(TS_{I \rightarrow J} - I) = 0.17$  eV, respectively. These results are graphically summarized in Fig. S4 of the SM [41]. We remark that in the final structure (J), while three stable C-C bonds are formed, the dislodged Si atom is still bound to the step edge and can hardly escape elsewhere. Nonetheless, this Si can undergo desorption from the step edge following the reaction pathway discussed in Sec. III A for the first Si desorption.

## C. C clustering after Si desorption

To complete our investigation, we focused on the process responsible for the clustering of C atoms, because this is the major process leading to the formation of graphene seeds. Clearly, this can occur only upon removal of several Si atoms. To start from a condition compatible with these requirements, the computational model we prepared has a wider area than our previous models described in the Methods section and used above. For this specific purpose, we removed 15 Si

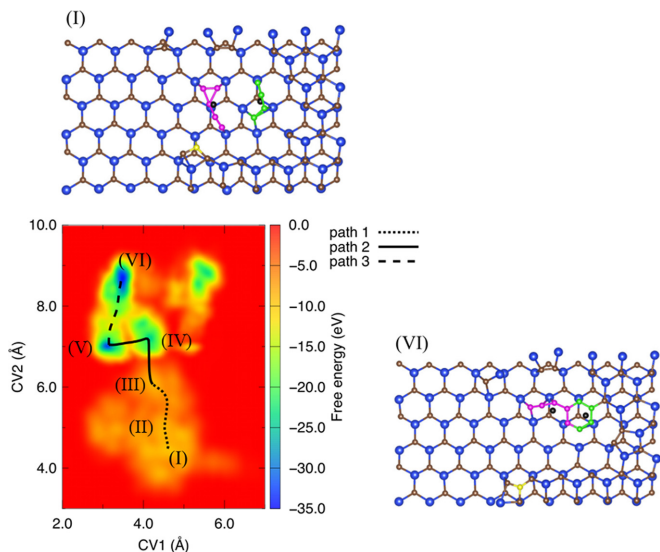


FIG. 4. Free-energy landscape (bottom left) and minimum free-energy reaction pathway (path1 + path2 + path3: dotted, solid, and dashed lines, respectively) for the clustering of carbon atoms. The labels from (I) to (VI) in the landscape indicate the positions of the (meta) stable configurations along the pathway. The free-energy profile along the identified pathway is given in Fig. S7 of the SM [41]. The stable configurations (I) and (VI) are shown in the top left and the bottom right, respectively. In (I),  $C_5$  and  $C_4$  clusters are highlighted with magenta and green spheres, respectively. Those clusters become a single cluster  $C_9$  in the final configuration (VI). The CV1 is the distance between the COM of  $C_5$  (left black sphere) and COM of  $C_4$  (right black sphere) and the CV2 is the distance between the COM of  $C_5$  and a C atom (yellow sphere).

atoms on the upper terrace near the step edge with a squared shape and allowed the system to relax and equilibrate in an unconstrained way by ordinary FPMD without any addition of CVs or other biasing methods. In about 1.6 ps, the system equilibrated into the structure (I) shown in Fig. 4 in which two specific C atom clusters spontaneously formed. These clusters, labeled as  $C_5$  and  $C_4$ , are highlighted in magenta and green, respectively, in this figure. They are still far from being graphene precursors and resemble more a sort of disordered polymer bound to the SiC substrate.

To investigate the actual formation of ordered C structures, we resorted to MTD simulation. Since in this case we focus on the C clustering process, the two CVs we selected to enhance this process are the distance between the COM of the  $C_5$  structure (left black sphere in Fig. 4) and the COM of the  $C_4$  structure (right black sphere), and the distance between the COM of  $C_5$  and the specific C atom indicated by a yellow sphere. Starting from the initial configuration (I), our MTD exploration of the free-energy landscape has been able to identify four metastable states, labeled as (II), (III), (IV), and (V), respectively, as shown in Fig. 4 and in Figs. S7 and S8 of the SM [41]. Each of them can be reached upon overcoming free-energy barriers that identify five transition states shown in Fig. S7 of the SM [41], namely,  $TS_{I \rightarrow II}$ ,  $TS_{II \rightarrow III}$ ,  $TS_{III \rightarrow IV}$ ,  $TS_{IV \rightarrow V}$ , and  $TS_{V \rightarrow VI}$ . Eventually, a final state (VI) in which nine C atoms near the step edge get together forming a  $C_9$

cluster is reached. This configuration is the deepest minimum of the free-energy surface and, as such, the most stable structure of the overall process. An inspection of the free-energy landscape for this reaction identifies the minimum free-energy pathway (path 1 + path 2 + path 3) and reveals that the various barriers to be overcome amount to

$$\begin{aligned}
 \Delta F(TS_{I \rightarrow II} - I) &= 0.06 \text{ eV}, \\
 \Delta F(TS_{II \rightarrow III} - II) &= 0.28 \text{ eV}, \\
 \Delta F(TS_{III \rightarrow IV} - III) &= 0.42 \text{ eV}, \\
 \Delta F(TS_{IV \rightarrow V} - IV) &= 1.32 \text{ eV}, \\
 \Delta F(TS_{V \rightarrow VI} - V) &= 1.42 \text{ eV}.
 \end{aligned}$$

As done in our previous analysis, we projected the pathway on a one-dimensional free-energy profile in Fig. S7 of the SM [41].

The five local minima identified along this pathway show that in the initial configuration (I), C-C chemical bonds are spontaneously formed upon regular dynamics at room temperature, along with a CCC triangular pattern. Metastable and transition-state configurations during this clustering reaction, shown in Fig. 4, and complementary Figs. S8 [41] and S9 [41] in the SM, provide a clear microscopic picture of the clustering of C atoms. In the stable state (I) which is attained through nonconstrained dynamical simulation upon Si removal at room temperature, the two clusters  $C_4$  and  $C_5$  coexist and many C-C bonds appear to have been formed. In the MTD simulation, the  $C_4$  and  $C_5$  gradually approach each other [(II) and (III)]. Then they start joining at the end carbons of each cluster [(IV)]. This caused the substantial energy gain of about 1.6 eV. After that the carbon clusters tend to be a ring shape [(V)] and in the final configuration we observe a six-membered ring [(VI)] with further energy gain of 1.2 eV.

The transition-state configurations shown in Fig. S9 of the SM [41] provide an atom-by-atom picture of the reaction mechanism. As shown above, the barriers from (I) to (IV) via (II) and (III) are small and the rate-determining barrier is 1.42 eV from (V) to (VI). The final configuration (VI) reached, is the deepest minimum of the free-energy surface. The total energy gain from (I) to (VI) is substantial, amounting to about 20.0 eV. This is a typical feature of a very stable system and the fact that this deep minimum corresponds to a fully formed graphene hexagonal structure is a fingerprint of an irreversible process. The metastable structures and transition states are shown in Figs. S8 [41] and S9 [41] of the SM.  $TS_{I \rightarrow II}$ , (II),  $TS_{II \rightarrow III}$ , and (III) are essentially identical to (I), which is not entirely unexpected in view of the fact that they are energetically very close, as shown in the free-energy profile of Fig. S7 in the SM [41]. In  $TS_{III \rightarrow IV}$  and (IV),  $C_5$  (magenta C) and  $C_4$  (green C) clusters arrange linearly. In  $TS_{IV \rightarrow V}$ , (V), and  $TS_{V \rightarrow VI}$ , the above linear C chain is attached to an edge C atom. The final configuration (VI) is the deepest minimum of the free-energy surface, corresponding to the realization of a  $C_6$  ring structure. This identifies the first step of the formation of a graphene layer.

The obtained structure (VI) is reached upon Si removal discussed in the case of the first and second Si desorption, with the energy barriers likely to be overcome at thermal decomposition temperature. The six-membered ring  $C_6$  cluster indeed appears there. We argue that the reaction found in the present simulations typifies the reactions for the graphene formation on the stepped SiC surface.

#### IV. CONCLUSIONS

In summary, to inspect the early stages of the process leading to the formation of graphene layers on a SiC(0001) surface, we have used forefront first-principles simulation methods complemented by enhanced sampling techniques to follow the reaction pathways and to provide a microscopic picture. Our simulations have shown that the desorption of a Si atom from a step edge and its subsequent migration to a stable site on the nearby terrace is an endothermic reaction. Yet, this step is an essential initial trigger to the process that eventually will lead to the formation of a graphene sheet. We have also found that a subsequent Si desorption leaves behind undercoordinated C atoms and this, in turn, triggers the formation of three stable C-C bonds via an exothermic reaction. This second step paves the route to the formation of a larger carbon structure at the SiC(0001) surface. Following the guidelines that these simulations indicate, we focused on the processes occurring upon desorption of several Si atoms. We have clarified how small C clusters formed at the exposed surface can merge into a larger structure presenting a C<sub>6</sub> ring, the expected seed of a graphenelike conformation. The extension of this carbon bond network realized in this way is accompanied by a remarkable energy gain, leading to an exothermic reaction and to a stable carbon structure precursor

of an actual graphene flake. This can provide a microscopic insight, still elusive to experimental probes, into this complex process, and the exothermic character of the reaction allows one to rationalize the rise of stable C-C bonds and the consequent graphene formation on the SiC step edge.

#### ACKNOWLEDGMENTS

This work was partly supported by the projects conducted under MEXT Japan named “Program for Promoting Research on the Supercomputer Fugaku (Multiscale simulations based on quantum theory toward the development of energy-saving next-generation semiconductor devices, project ID JPMXP1020200205). The JSPS grants-in-aid (Grant No. 18H03873) also supports the present work. Computations were performed with the resources provided by HPCI System (Project IDs: hp200122, hp210170, and hp220168) and by Supercomputer Center at Institute for Solid State Physics, University of Tokyo and at Institute for Molecular Sciences, National Institute of Natural Sciences. M.B. acknowledges the HPC Center at the University of Strasbourg funded by the Equipex Equip@Meso and the CPER Alsacalcul/Big Data, and the Grand Equipement National de Calcul Intensif (GENCI) under allocations DARI A0100906092 and A0120906092.

- 
- [1] J. C. Slonczewski and P. R. Weiss, Band structure of graphite, *Phys. Rev.* **109**, 272 (1958).
- [2] T. Ando and Y. Uemura, Theory of quantum transport in a two-dimensional electron system under magnetic fields. I. Characteristics of level broadening and transport under strong fields, *J. Phys. Soc. Jpn.* **36**, 959 (1974).
- [3] A. K. Geim and K. Novoselov, The rise of graphene, *Nat. Mater.* **6**, 183 (2007).
- [4] S. V. Morozov, K. S. Novoselov, M. I. Katsnelson, F. Schedin, D. C. Elias, J. A. Jaszczak, and A. K. Geim, Giant Intrinsic Carrier Mobilities in Graphene and Its Bilayer, *Phys. Rev. Lett.* **100**, 016602 (2008).
- [5] K. I. Bolotin, K. J. Sikes, Z. Jiang, M. Klima, G. Fudenberg, J. Hone, P. Kim, and H. L. Stormer, Ultrahigh electron mobility in suspended graphene, *Solid State Commun.* **146**, 351 (2008).
- [6] H. C. Schniepp, J. L. Li, M. J. McAllister, H. Sai, M. Herrera-Alonso, and D. H. Adamson, Functionalized single graphene sheets derived from splitting graphite oxide, *J. Phys. Chem. B* **110**, 8535 (2006).
- [7] N. Liu, F. Luo, H. Wu, Y. Liu, C. Zhang, and J. Chen, One-step ionic-liquid-assisted electrochemical synthesis of ionic-liquid-functionalized graphene sheets directly from graphite, *Adv. Funct. Mater.* **18**, 1518 (2008).
- [8] G. Wang, B. Wang, J. Park, Y. Wang, B. Sun, and J. Yao, Highly efficient and large-scale synthesis of graphene by electrolytic exfoliation, *Carbon* **47**, 3242 (2009).
- [9] N. Mishra, J. Boeckl, N. Motta, and F. Iacopi, Graphene growth on silicon carbide: A Review, *Phys. Status Solidi A* **213**, 2277 (2016).
- [10] C. Berger, Z. Song, X. Li, X. Wu, N. Brown, C. Naud, D. Mayou, T. Li, J. Hass, A. N. Marchenkov, E. H. Conrad, P. N. First, and W. A. de Heer, Electronic confinement and coherence in patterned epitaxial graphene, *Science* **312**, 1191 (2006).
- [11] J. Borysiuk, J. Soltys, R. Bożek, J. Piechota, S. Krukowski, W. Strupiński, J. M. Baranowski, and R. Stepniowski, Role of structure of C-terminated 4H-SiC(0001) surface in growth of graphene layers: Transmission electron microscopy and density functional theory studies, *Phys. Rev. B* **85**, 045426 (2012).
- [12] W. Norimatsu and M. Kusunoki, Transitional structures of the interface between graphene and 6H-SiC(0001), *Chem. Phys. Lett.* **468**, 52 (2009).
- [13] K. V. Emtsev, A. Bostwick, K. Horn, J. Jobst, G. L. Kellogg, L. Ley, J. L. McChesney, T. Ohta, S. A. Reshanov, J. Röhrl, E. Rotenberg, A. K. Schmid, D. Waldmann, H. B. Weber, and T. Seyller, Towards wafer-size graphene layers by atmospheric pressure graphitization of silicon carbide, *Nat. Mater.* **8**, 203 (2009).
- [14] W. Norimatsu and M. Kusunoki, Formation process of graphene on SiC (0001), *Phys. E* **42**, 691 (2010).
- [15] W. Chen, H. Xu, L. Liu, X. Gao, D. Qi, G. Peng, S. C. Tan, Y. Feng, K. P. Loh, and A. T. S. Wee, Atomic structure of the 6H-SiC(0001) nanomesh, *Surf. Sci.* **596**, 176 (2005).
- [16] M.-H. Tsai, C. S. Chang, J. D. Dow, and I. S. T. Tsong, Electronic contributions to scanning-tunneling-microscopy images of an annealed  $\beta$ -SiC(111) surface, *Phys. Rev. B* **45**, 1327 (1992).
- [17] T. Seyller, K. Emtsev, K. Gao, F. Speck, L. Ley, A. Tadich, L. Broekman, J. Riley, R. Leckey, O. Rader, A. Varykhalov, and A. Shikin, Structural and electronic properties of graphite layers grown on SiC(0001), *Surf. Sci.* **600**, 3906 (2006).
- [18] A. Charrier, A. Coati, T. Argunova, F. Thibaudau, Y. Garreau, R. Pinchaux, I. Forbeaux, J.-M. Debever, M. Sauvage-Simkin, and J.-M. Themlin, Solid-state decomposition of silicon carbide



- for growing ultra-thin heteroepitaxial graphite films, *J. Appl. Phys.* **92**, 2479 (2002).
- [19] E. Rollings, G.-H. Gweon, S. Zhou, B. Mun, J. McChesney, B. Hussain, A. Fedorov, P. First, W. de Heer, and A. Lanzara, Synthesis and characterization of atomically thin graphite films on a silicon carbide substrate, *J. Phys. Chem. Solids* **67**, 2172 (2006).
- [20] P. Lauffer, K. V. Emtsev, R. Graupner, Th. Seyller, L. Ley, S. A. Reshanov, and H. B. Weber, Atomic and electronic structure of few-layer graphene on SiC(0001) studied with scanning tunneling microscopy and spectroscopy, *Phys. Rev. B* **77**, 155426 (2008).
- [21] M. Hupalo, E. H. Conrad, and M. C. Tringides, Growth mechanism for epitaxial graphene on vicinal 6H-SiC(0001) surfaces: A scanning tunneling microscopy study, *Phys. Rev. B* **80**, 041401(R) (2009).
- [22] W. Zhang and A. C. T. van Duin, Atomistic-scale simulations of the graphene growth on a silicon carbide substrate using thermal decomposition and chemical vapor deposition, *Chem. Mater.* **32**, 8306 (2020).
- [23] M. Morita, W. Norimatsu, H.-J. Qian, S. Irle, and M. Kusunoki, Atom-by-atom simulations of graphene growth by decomposition of SiC (0001): Impact of the substrate steps, *Appl. Phys. Lett.* **103**, 141602 (2013).
- [24] M. Inoue, H. Kageshima, Y. Kangawa, and K. Kakimoto, First-principles calculation of 0<sup>th</sup>-layer graphene-like growth of C on SiC(0001), *Phys. Rev. B* **86**, 085417 (2012).
- [25] S. Takamoto, T. Yamasaki, J. Nara, T. Ohno, C. Kaneta, A. Hatano, and S. Izumi, Atomistic mechanism of graphene growth on a SiC substrate: Large-scale molecular dynamics simulations based on a new charge-transfer bond-order type potential, *Phys. Rev. B* **97**, 125411 (2018).
- [26] W. Kohn and L. J. Sham, Self-consistent equations including exchange and correlation effects, *Phys. Rev.* **140**, A1133 (1965).
- [27] S. Kim, J. Ihm, H. J. Choi, and Y.-W. Son, Origin of Anomalous Electronic Structures of Epitaxial Graphene on Silicon Carbide, *Phys. Rev. Lett.* **100**, 176802 (2008).
- [28] F. Varchon, P. Mallet, J.-Y. Veuillen, and L. Magaud, Ripples in epitaxial graphene on the Si-terminated SiC(0001) surface, *Phys. Rev. B* **77**, 235412 (2008).
- [29] H. Kageshima, H. Hibino, H. Yamaguchi, and M. Nagase, Theoretical study on epitaxial graphene growth by Si sublimation from SiC(0001) surface, *Jpn. J. Appl. Phys.* **50**, 095601 (2011).
- [30] H. Kageshima, H. Hibino, and S. Tanabe, The physics of epitaxial graphene on SiC(0001), *J. Phys.: Condens. Matter* **24**, 314215 (2012).
- [31] F. Imoto, J.-I. Iwata, M. Boero, and A. Oshiyama, Microscopic mechanisms of initial formation process of graphene on SiC(0001) surfaces: Selective Si desorption from step edges, *J. Phys. Chem. C* **121**, 5041 (2017).
- [32] K. Sawada, J.-I. Iwata, and A. Oshiyama, Magic angle and height quantization in nanofacets on SiC(0001) surfaces, *Appl. Phys. Lett.* **104**, 051605 (2014).
- [33] K. Sawada, J.-I. Iwata, and A. Oshiyama, Spontaneous appearance of a low-dimensional magnetic electron system on semiconductor nanostructures, *Phys. Rev. B* **93**, 235421 (2016).
- [34] K. Seino and A. Oshiyama, Energetics of the surface step and its morphology on the 3C-SiC(111) surface clarified by the density-functional theory, *Appl. Phys. Express* **13**, 015506 (2020).
- [35] K. Seino and A. Oshiyama, Density functional calculations for structures and energetics of atomic steps and their implication for surface morphology on Si-face SiC polar surfaces, *Phys. Rev. B* **101**, 195307 (2020).
- [36] R. Car and M. Parrinello, Unified Approach for Molecular Dynamics and Density-Functional Theory, *Phys. Rev. Lett.* **55**, 2471 (1985).
- [37] CPMD, copyright IBM Corp. (1990–2022) and MPI für Festkörperforschung Stuttgart (1997–2001), [www.cpmc.org/](http://www.cpmc.org/).
- [38] A. Laio and M. Parrinello, Escaping free-energy minima, *Proc. Natl. Acad. Sci. USA* **99**, 12562 (2002).
- [39] M. Iannuzzi, A. Laio, and M. Parrinello, Efficient Exploration of Reactive Potential Energy Surfaces using Car-Parrinello Molecular Dynamics, *Phys. Rev. Lett.* **90**, 238302 (2003).
- [40] K. Shiraiishi, New slab-model approach for electronic structure calculation of polar semiconductor surface, *J. Phys. Soc. Jpn.* **59**, 3455 (1990).
- [41] See Supplemental Material at <http://link.aps.org/supplemental/10.1103/PhysRevMaterials.6.093403> for additional figures and results discussed in the text.
- [42] R. J. Magyar, S. Root, and T. R. Mattsson, Equations of state for mixtures: Results from density-functional (DFT) simulations compared to high accuracy validation experiments on Z, *J. Phys.: Conf. Ser.* **500**, 162004 (2014).
- [43] R. Rousseau, M. Boero, M. Bernasconi, M. Parrinello, and K. Terakura, *Ab Initio* Simulation of Phase Transitions and Dissociation of H<sub>2</sub>S at High Pressure, *Phys. Rev. Lett.* **85**, 1254 (2000).
- [44] S. Nosé, A molecular dynamics method for simulations in the canonical ensemble, *Mol. Phys.* **52**, 255 (1984).
- [45] S. Nosé, A unified formulation of the constant temperature molecular dynamics methods, *J. Chem. Phys.* **81**, 511 (1984).
- [46] W. G. Hoover, Canonical dynamics: Equilibrium phase-space distributions, *Phys. Rev. A* **31**, 1695 (1985).
- [47] G. J. Martyna, M. L. Klein, and M. Tuckerman, Nosé-Hoover chains: The canonical ensemble via continuous dynamics, *J. Chem. Phys.* **97**, 2635 (1992).
- [48] J. P. Perdew, K. Burke, and M. Ernzerhof, Generalized Gradient Approximation Made Simple, *Phys. Rev. Lett.* **77**, 3865 (1996).
- [49] S. Grimme, Accurate description of van der Waals complexes by density functional theory including empirical corrections, *J. Comput. Chem.* **25**, 1463 (2004).
- [50] N. Troullier and J. L. Martins, Efficient pseudopotentials for plane-wave calculations, *Phys. Rev. B* **43**, 1993 (1991).
- [51] A. Barducci, M. Bonomi, and M. Parrinello, Metadynamics, *WIREs Comput. Mol. Sci.* **1**, 826 (2011), and references therein.
- [52] M. Parrinello, Breviarium de motu simulatio ad atomos pertinenti, *Isr. J. Chem.* **62**, e202100105 (2022).
- [53] P. Raiteri, A. Laio, F. L. Gervasio, C. Micheletti, and M. Parrinello, Efficient reconstruction of complex free energy landscapes by multiple walkers metadynamics, *J. Phys. Chem. B* **110**, 3533 (2006).